A family of edge-centered finite volume schemes for heterogeneous and anisotropic diffusion problems on unstructured meshes

Ziqi Liu[a], Shuai Miao[b], Zhimin Zhang[c,d,*]

[a]*Department of Mathematical Sciences, Tsinghua University, Beijing 100084, PR China*
[b]*Graduate School of China Academy of Engineering Physics, Beijing, 100088, PR China*
[c]*Applied and Computational Mathematics Division, Beijing Computational Science Research Center, Beijing 100193, China*
[d]*Department of Mathematics, Wayne State University, Detroit, Michigan 48202, United States of America*

Abstract

We present a family of edge-centered finite volume schemes for steady-state diffusion problems on general unstructured polygonal meshes. These schemes are locally conservative with respect to the dual mesh and have only edge-centered unknowns with no extra auxiliary variable. A general form of edge-centered finite volume scheme based on linearity-preserving criterion is proposed, and two specific schemes (ECS-I and ECS-II) are constructed. In particular, ECS-II derives a symmetric and positive definite matrix, and its coercivity can be rigorously demonstrated. The ECS-II is unconditionally stable in any star-shaped mesh. Besides, the relationship between edge-centered schemes and the finite volume element method with Crouzeix-Raviart element and the finite difference method with X-shaped stencil is discussed. Numerical experiments indicate that edge-centered schemes have optimal convergence rate and are robust even for highly anisotropic problems and distorted meshes.

Keywords: edge-centered scheme; unstructured mesh; diffusion equation; symmetric and coercive

1. Introduction

Anisotropic and heterogeneous diffusion problems arise in a wide range of scientific fields, such as Navier-Stokes equations [1, 2], petroleum reservoir simulation [3, 4, 5], semiconductor device design [6], etc. Therefore, it is important to design a robust and accurate numerical scheme for solving diffusion problems. There are following difficulties in designing the scheme. Firstly, heterogeneous means that the diffusion tensor may be

*Corresponding author.
Email addresses: liu-zq21@mails.tsinghua.edu.cn (Ziqi Liu), miaoshuai18@gscaep.ac.cn (Shuai Miao), zmzhang@csrc.ac.cn (Zhimin Zhang)

severely discontinuous. This will lead to the loss of the regularity of the solution, which limits the use of higher-order methods. Secondly, for anisotropic problems, the direction of diffusion and the mesh division are inconsistent. Furthermore, since it is very difficult to generate structured meshes on complex regions, the scheme needs to adapt to unstructured and highly distorted meshes. Finally, to obtain a physical solution, the scheme should be locally conservative.

In recent decades, a large number of numerical methods have emerged. Among them, finite volume method is widely used because of its conservation characteristics and strong adaptability to geometry. These schemes can be roughly divided into cell-centered schemes, vertex-centered schemes, mimetic schemes and other schemes. Most of classic schemes, such as the multi-point flux approximation scheme (MPFA) [7, 8], and the nine-point scheme (also called the diamond scheme) [9, 10] are cell-centered schemes. Usually, vertex-centered schemes need to be implemented by dividing dual meshes, and the local conservation law holds with respect to dual meshes. In recent years, some other vertex-centered finite volume schemes [11, 12] have been developed. Based on the linearity-preserving criterion, a vertex-centered scheme is designed in [13]. Particularly, linear equations derived from this scheme are symmetric and positive definite (SPD). There are also some finite volume schemes have not only the cell-centered unknowns or vertex-centered unknowns e.g., mimetic schemes [14, 15, 16, 17] have both cell-centered unknowns and edge (or edge-flux) unknowns, and adds conservation conditions to the linear equations to establish the equations of edge (or edge-flux) unknowns. Besides, the DDFV schemes [18, 19] have cell-centered unknowns and vertex unknowns simultaneously.

Although the research on edge-centered finite volume schemes is rare, there are some researches on finite volume schemes that define unknowns only on the faces (3D) or edges (2D) of meshes [20]. Back in 1999, a Crouzeix-Raviart finite volume element scheme [21] was proposed and analyzed strictly. In [22], an edge-based finite volume scheme is applied on the groundwater simulation. In recent years, a face-centered finite volume (FCFV) scheme for elliptic equations [23, 24] and a locking-free FCFV scheme for linear elastostatics equations [25] have been proposed. As for compressible fluids simulation, a non-oscillatory FCFV scheme [26] was proposed. There is also face centered scheme [27] for automatic mesh refinement. However, the linear equations formed by all the above schemes are not SPD, which brings great difficulties to the theoretical analysis.

In practical calculations, the diffusion phenomenon is usually coupled with fluid dynamics. Thus, there are eager requirement for a well-posed edge-centered finite volume scheme for diffusion equations. Compared with the cell-centered and vertex-centered schemes, most of researches e.g., [24, 25] indicate that edge-centered schemes are more robust and accurate on distorted meshes. Furthermore, compared with the mimetic schemes, the edge-centered schemes have fewer unknowns, so smaller scale linear equations is derived. Meanwhile, in the edge-centered schemes, the conservation condition is strictly satisfied. Based on the above overview, we construct a family of linear edge-centered finite volume schemes for diffusion problems. The main features of schemes can be summarized as follows:

- One of them (ECS-II) leads to SPD linear systems.
- They allow discontinuities and anisotropic diffusion tensors.
- They have only edge-centered unknowns without extra auxiliary variable.
- They all reduce to a CR-FVEM scheme on triangular meshes.
- They have approximately optimal convergence order for L^2 and L^∞ error even in some extreme cases.

The rest of this paper is organized as follows. In section 2, we introduce the governing equation of the diffusion problem, the construction of the dual mesh and some notations. In section 3, we propose a general form and construct two edge-centered schemes (ECS-I and ECS-II) based on the linearity-preserving criterion. In section 4, the coercivity and stability of the scheme ECS-II are studied. Some special cases are also analysed in section 4. Numerical results are given in section 5 to show the performance of new schemes on some challenging problems. Finally, the conclusions and future works are summarized in section 6.

2. Problems and notations

2.1. Steady-state diffusion problems

We consider the steady-state diffusion problem

$$\begin{cases} -\nabla \cdot (\Lambda \nabla u) = f & \boldsymbol{x} \in \Omega, \\ u = g & \boldsymbol{x} \in \partial\Omega. \end{cases} \tag{1}$$

where $\Omega \subset \mathbb{R}^2$ is an open bounded polygonal domain with boundary $\partial\Omega$, $u(\boldsymbol{x})$ is the unknown function, $f(\boldsymbol{x}) \in L^2(\Omega)$ is the source term, $g(\boldsymbol{x})$ defined on $\partial\Omega$ is the boundary data, $\Lambda(\boldsymbol{x})$ is the diffusion tensor. Here, Λ is symmetric and there exits two positive number $\underline{\lambda}, \overline{\lambda}$ satisfying

$$\underline{\lambda}\, \|\boldsymbol{v}\|^2 \leq \boldsymbol{v}^T\, \Lambda(\boldsymbol{x})\, \boldsymbol{v} \leq \overline{\lambda}\, \|\boldsymbol{v}\|^2, \quad \forall\, \boldsymbol{v} \in \mathbb{R}^2, \forall\, \boldsymbol{x} \in \Omega.$$

In the problem, Λ is piecewise continuous but possibly discontinuous on Ω, which will result in the loss of regularity of the solution u. We can only get $u \in H^1(\Omega)$ and $\Lambda \nabla u \in H^{\mathrm{div}}(\Omega)$, and cannot obtain higher-order regularity.

2.2. Primary and dual mesh

The construction of the prime and dual meshes is slightly different from traditional meshes. Consider a mesh $\mathcal{M}$ composed of a finite number of disjoint polygonal cells. With each cell in the mesh, we associate one point which is called cell center. We assume that each cell is star-shaped with respect to its center, which means that all lines connecting

its center and vertexes are contained by the cell. In this paper, we chose the centroid of the cell as its center. Based on the prime mesh $\mathcal{M}$, the line connecting a cell center and its surrounding vertex is called the dual edge. For a certain edge of $\mathcal{M}$, if the edge is not on the boundary $\partial\Omega$, then is surrounded by four dual edges. The area surrounded by these four dual edges is called the edge control volume. For an edge of $\mathcal{M}$ that located on the boundary, the corresponding edge control volume is surrounded by the edge itself and two adjacent dual edges. Edge control volumes are combined to form the dual mesh $\mathcal{M}^*$. Vertexes of $\mathcal{M}^*$ are the union of vertexes and cell centers of the prime mesh $\mathcal{M}$, edges of $\mathcal{M}^*$ are the dual edges and cells of $\mathcal{M}^*$ are edge control volumes. Figure 1a shows the polygonal prime mesh $\mathcal{M}$ and the dual mesh $\mathcal{M}^*$ on a square domain. Without misleading, a cell of $\mathcal{M}$ or the center of corresponding cell are all denoted by K, an edge of $\mathcal{M}$ or the midpoint of corresponding edge or the corresponding edge control volume are all denoted by E, a vertex of $\mathcal{M}$ is denoted by P, and the dual edge in $\mathcal{M}^*$ is denoted by σ. $\boldsymbol{n}_{E,\sigma}$ denotes the unit outer normal on the line σ of edge control volume E. If σ is the common edge of E_1 and E_2, there holds $\boldsymbol{n}_{E_1,\sigma} = -\boldsymbol{n}_{E_2,\sigma}$. When not mentioned, $\boldsymbol{n}_\sigma$ represents the normal vector of σ with anti-clockwise direction. For a certain polygon cell $K \in \mathcal{M}$ with m_K edges, as shown in Figure 1b, the nodes is numbered anti-clockwise as $P_1, P_2, \cdots, P_{m_K}$. We denote $P_{m_K+1} = P_1, P_0 = P_{m_K}$. Edges in dual edges are numbered similarly. The edge E_i connects P_i and P_{i+1} and the line σ_i connects K and P_i. The coordinates of the vertex P_i is denoted by $\boldsymbol{x}_i = (x_i, y_i)^T$ and the coordinates of the edge midpoint E and the the cell center K is denoted by $\boldsymbol{x}_E$ and $\boldsymbol{x}_K$ respectively.

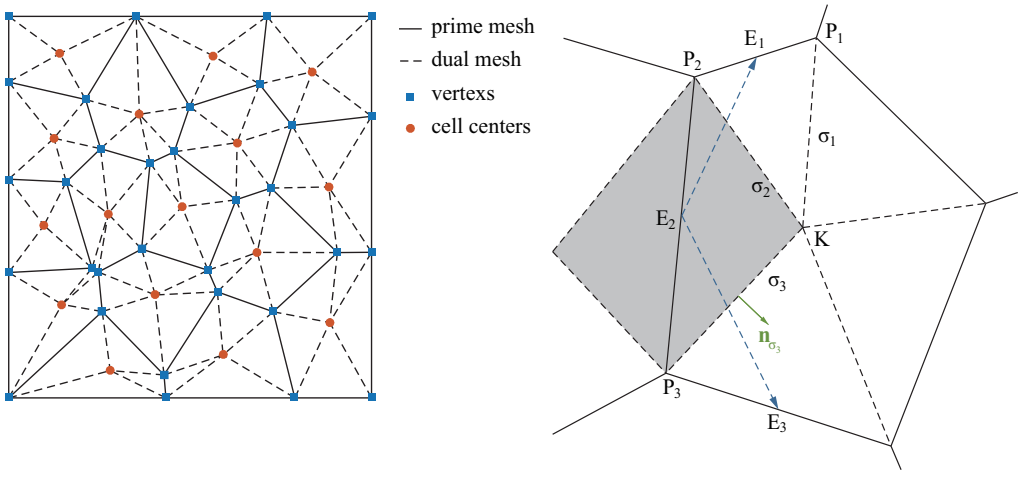

(a) The prime and dual mesh (b) notations and the stencil

Figure 1: Meshes and notations

3. Construction of the scheme

3.1. A general form of edge-centered finite volume scheme

By integrating the problem Eq. (1) over the edge control volume E, we obtain

$$-\int_E \nabla \cdot (\Lambda \nabla u)\ \mathrm{d}\boldsymbol{x} = \sum_{\sigma \in \sigma(E)} \mathcal{F}_{E,\sigma} = \int_E f\ \mathrm{d}\boldsymbol{x}, \tag{2}$$

where the continuous normal flux $\mathcal{F}_{E,\sigma}$ of σ is defined by

$$\mathcal{F}_{E,\sigma} = -\int_\sigma (\Lambda \nabla u) \cdot \boldsymbol{n}_{E,\sigma}\ \mathrm{d}s,$$

and $\sigma(E)$ represents the set of dual edges surrounding the edge control volume E.

For two adjacent edge control volumes E_1 and E_2 with σ as the common edge, by continuity of the normal flux component, we have

$$\mathcal{F}_{E_1,\sigma} = -\mathcal{F}_{E_2,\sigma}.$$

Next, we construct the flux approximation F_σ on the dual edge σ using the edge unknowns. As shown in Figure 1b, for a polygon K in prime mesh, we put all flux on dual edges $\{\sigma_i\}$ into a vector and manipulate them together. We denote that

$$\mathbf{F}_K = (F_{\sigma_i},\ i = 1, 2, \cdots, m_K)^T, \qquad \delta\mathbf{U}_K = (u(E_i) - u(E_{i-1}),\ i = 1, 2, \cdots, m_K)^T, \tag{3}$$

where $\mathbf{F}_K$ is the vector of the flux approximations, and $\delta\mathbf{U}_K$ is the vector of differences of edge unknowns. In a linear scheme, all flux are approximated by a linear combination of the values of the solution on the middle points $\{E_i\}$. Considering that the formula should be exact for constant solutions, which means that the flux should be zero when the solution is constant. Then the flux is approximated by

$$\mathbf{F}_K = A_K\, \delta\mathbf{U}_K, \tag{4}$$

where A_K is called cell matrix of size $m_K \times m_K$.

Here, we introduce the linearity-preserving criterion for the construction of the cell matrix A_K. The linearity-preserving criterion means that our scheme should be exact for piecewise linear solutions whose diffusion tensor is piecewise constant with respect to the primary mesh. All derivations below are based on the assumption that the diffusion coefficient is piecewise constant and the solution is piecewise linear.

We construct a linearity-preserving scheme and expect it to have second-order accuracy. By choosing the solution as $u(\boldsymbol{x}) = x$ and $u(\boldsymbol{x}) = y$, we can get the scheme satisfies the linearity-preserving criterion if and only if

$$N_K\, \Lambda_K = A_K\, X_K, \tag{5}$$

where

$$N_K = (-|\sigma|\, \boldsymbol{n}_{\sigma_i}^T,\ i = 1, 2, \cdots, m_K)^T, \qquad X_K = ((\boldsymbol{x}_{E_i} - \boldsymbol{x}_{E_{i-1}})^T,\ i = 1, 2, \cdots, m_K), \quad (6)$$

here N_K and X_K are two $m_K \times 2$ matrices, $\boldsymbol{x}_{E_i}$ represents the coordinates of the midpoint of the edge E_i and Λ_K is the constant approximation of the diffusion tensor on cell K. In this paper, Λ_K is chosen as the value of $\Lambda(\boldsymbol{x})$ at the cell center.

The critical part of an edge-centered scheme is to construct the cell matrix A_K such that the linearity-preserving criterion is fulfilled. In Eq. (5), there are m_K^2 unknowns in A_K but only $2m_K$ equations, so we have many choices of A_K. Here we are interested in the construction of A_K with other properties, such as SPD or local stencil. Here we give two following constructions. After obtained the flux approximation, the final numerical scheme writes

$$\sum_{\sigma \in \sigma(E)} F_{E,\sigma} = \int_E f \ \mathrm{d}\boldsymbol{x}. \quad (7)$$

3.2. A scheme based on vector decomposition (ECS-I)

In this subsection, we construct an edge-centered scheme (ECS-I) with local stencil satisfying linearity-preserving criterion. Here we construct the flux approximation based on vector decomposition without explicitly establishing the cell matrix A_K.

For a linear solution with a constant diffusion tensor on a certain polygon K, for example, when we approximating the flux $\mathcal{F}_{E_2,\sigma_2}$, we have

$$F_{E_2,\sigma_2} = -\int_{\sigma_2} (\Lambda_K \nabla u) \cdot \boldsymbol{n}_{E_2,\sigma_2} \ \mathrm{d}s = -|\sigma_2|\, (\Lambda_K^T\, \boldsymbol{n}_{E_2,\sigma_2}) \cdot \nabla u. \quad (8)$$

As shown in Figure 1b we can decompose the vector $|\sigma_2|\, (\Lambda_K^T\, \boldsymbol{n}_{E_2,\sigma_2})$ as the linear combination of vector $\overrightarrow{E_2E_1}$ and $\overrightarrow{E_2E_3}$, that is

$$|\sigma_2|\, \Lambda_K^T\, \boldsymbol{n}_{E_2,\sigma_2} = \alpha_- \overrightarrow{E_2E_1} + \alpha_+ \overrightarrow{E_2E_3}. \quad (9)$$

For a linear solution u, the gradient of u along the direction $\overrightarrow{E_2E_1}$ and $\overrightarrow{E_2E_3}$ can be written as

$$\nabla u \cdot \overrightarrow{E_2E_1} = u(E_1) - u(E_2), \qquad \nabla u \cdot \overrightarrow{E_2E_3} = u(E_3) - u(E_2).$$

Then we can get the flux approximation for piecewise linear solution

$$F_{E_2,\sigma_2} = \alpha_- \left(u(E_2) - u(E_1)\right) + \alpha_+ \left(u(E_2) - u(E_3)\right)$$

where α_-, α_+ is given by vector decomposition Eq. (9).

For edge control volume E_1, we can get the flux approximation F_{E_1,σ_2} similarly. Note that the flux approximation F_{E_1,σ_2} is represented by $u(E_0)$, $u(E_1)$ and $u(E_2)$, and its stencil is usually different from F_{E_2,σ_2}. Now we have two flux approximations, in order

to satisfy the local conservation law, we should combine them into one. Since that both flux approximation satisfy the linearity-preserving criterion, we take a simple average of the two approximations and get the final flux. Note that the direction relationship $\boldsymbol{n}_{\sigma_2} = \boldsymbol{n}_{E_1,\sigma_2} = -\boldsymbol{n}_{E_2,\sigma_2}$, the final flux writes

$$F_{\sigma_2} = \frac{1}{2}(F_{E_1,\sigma_2} - F_{E_2,\sigma_2}).$$

3.3. A scheme based on matrix stabilization (ECS-II)

In this subsection, we use the special property of polygonal mesh to construct SPD cell matrix to meet the linearity-preserving criterion. The scheme derived here is called ECS-II.

Firstly, we demonstrate the geometry relationship in polygons.

Lemma 1 (Shoelace Formula)**.** *Consider a polygon K with m_K edges, whose nodes $\boldsymbol{x}_1 = (x_1, y_1), \boldsymbol{x}_2 = (x_2, y_2), \cdots, \boldsymbol{x}_{m_K} = (x_{m_K}, y_{m_K})$ is ranged anti-clockwise, then the area of K is*

$$|K| = \frac{1}{2}\sum_{i=1}^{m_K}(x_i\, y_{i+1} - x_{i+1}\, y_i). \tag{10}$$

With the help of Lemma 1 we can get the relationship between N_K and X_K.

Theorem 1. *For arbitrary polygon K, two matrices N_K and X_K are defined in Eq.* (6)*. Then we have*

$$N_K^T\, X_K = |K|\, I_2, \tag{11}$$

where I_2 represents the 2×2 identity matrix.

Proof. For a polygon K with m_K nodes $\boldsymbol{x}_1 = (x_1, y_1), \boldsymbol{x}_2 = (x_2, y_2), \cdots, \boldsymbol{x}_{m_K} = (x_{m_K}, y_{m_K})$ and center $\boldsymbol{x}_K$, we have

$$|\sigma_i|\boldsymbol{n}_{\sigma_i} = \mathcal{R}\,(\boldsymbol{x}_i - \boldsymbol{x}_K), \qquad \boldsymbol{x}_{E_i} - \boldsymbol{x}_{E_{i+1}} = \frac{1}{2}\,(\boldsymbol{x}_{i-1} - \boldsymbol{x}_{i+1}), \qquad \mathcal{R} = \begin{pmatrix} 0 & 1 \\ -1 & 0 \end{pmatrix},$$

where $\mathcal{R}$ represents the rotation matrix and $\boldsymbol{x}_{E_i}$ represents the coordinates of the midpoint of the edge E_i.

Using the definition of N_K and X_K, we have

$$N_K^T\, X_K = \sum_{i=1}^{m_K} |\sigma_i|\, \boldsymbol{n}_{\sigma_i}\, (\boldsymbol{x}_{E_i} - \boldsymbol{x}_{E_{i+1}})^T = \frac{1}{2}\sum_{i=1}^{m_K} \mathcal{R}\,(\boldsymbol{x}_i - \boldsymbol{x}_K)\,(\boldsymbol{x}_{i-1} - \boldsymbol{x}_{i+1})^T.$$

Since the formula is translation invariant, we can shift the center of the polygon to coordinate origin. Then we have

$$N_K^T\, X_K = \frac{1}{2}\sum_{i=1}^{m_K} \mathcal{R}\,\boldsymbol{x}_i\,(\boldsymbol{x}_{i-1} - \boldsymbol{x}_{i+1})^T - \frac{1}{2}\,\boldsymbol{x}_K \sum_{i=1}^{m_K} \mathcal{R}\,(\boldsymbol{x}_{i-1} - \boldsymbol{x}_{i+1})^T = \frac{1}{2}\sum_{i=1}^{m_K} \mathcal{R}\,\boldsymbol{x}_i\,(\boldsymbol{x}_{i-1} - \boldsymbol{x}_{i+1})^T.$$

Expand the above into component form, we can obtain

$$N_K^T X_K = \frac{1}{2}\sum_{i=1}^{m_K}\begin{pmatrix} y_i\,(x_{i-1}-x_{i+1}) & y_i\,(y_{i-1}-y_{i+1}) \\ x_i\,(x_{i+1}-x_{i-1}) & x_i\,(y_{i+1}-y_{i-1}) \end{pmatrix}$$

Using Lemma 1, we have

$$|K| = \frac{1}{2}\sum_{i=1}^{m_K} y_i\,(x_{i-1}-x_{i+1}) = \frac{1}{2}\sum_{i=1}^{m_K} x_i\,(y_{i+1}-y_{i-1}),$$

and

$$\sum_{i=1}^{m_K} x_i\,(x_{i-1}-x_{i+1}) = \sum_{i=1}^{m_K} y_i\,(y_{i+1}-y_{i-1}) = 0.$$

Finally we can get

$$N_K^T X_K = \begin{pmatrix} |K| & 0 \\ 0 & |K| \end{pmatrix} = |K|\,I_2.$$

Remark 1. *This theorem can be seen as a extension of the Lemma 3.1 in [13], but there are still some essential differences between them. The formula plays an important role in constructing a SPD cell matrix.*

Multiplying Eq. (11) *with* $\frac{1}{|K|}\,N_K^T\,\Lambda_K$*, and comparing the result with Eq.* (5)*, we can find that if we choose*

$$A_K = \frac{1}{|K|}\,N_K\,\Lambda_K\,N_K^T,$$

the linearity-preserving condition will be satisfied. Nevertheless, cell matrix A_K *of this form is symmetric but only semi-positive definite. Motivated by [13], we add a stabilization term and get*

$$A_K = \frac{1}{|K|}\,N_K\,\Lambda_K\,N_K^T + \gamma_K\,C_K, \quad \textit{with} \quad C_K = I_K - X_K\,(X_K^T\,X_K)^{-1}\,X_K^T, \tag{12}$$

where I_K *is a* $m_K \times m_K$ *identity matrix and* γ_K *is a positive number called stabilization parameter. The matrix* C_K *serves as the stabilization term.*

The following theorem ensures the stabilization term is well-defined and the scheme with stabilization term is still linearity-preserving.

Theorem 2. *For arbitary polygon* K*,* X_K *is defined in Eq.* (6) *and* C_K *is defined in Eq.* (12)*. Then* $X_K^T\,X_K$ *is non-singular and the column vectors of* C_K *span the null space of* X_K *a.e.* $C_K\,X_K = 0$*.*

Connecting the midpoints of neighbor edges in polygon K*, we can get a new polygon. The Theorem 2 can be proved by using (Theorem 3.1 and Theorem 3.2 in [28]) on the new polygon.*

4. Analysis of edge-centered schemes

4.1. Coercivity analysis

In convergence analysis of finite volume schemes, the critical part is to demonstrate the coercivity. Basing on the construction of ECS-II, we have following theorems.

Lemma 2. *The cell matrix A_K defined in Eq. (12) is SPD, moreover*

$$\underline{\rho}_K \|v\|^2 \leq v^T A_K v \leq \overline{\rho}_K \|v\|^2, \quad \forall\, v \in \mathbb{R}^{m_K},\ \forall\, K \in \mathcal{M}. \tag{13}$$

where $\underline{\rho}_K$ and $\overline{\rho}_K$ are positive constants independent of the mesh size.

The proof is similar to Theorem 4.1 in [28], so omit here.

Theorem 3 (Coercivity of ECS-II)**.** *Assume $g = 0$. Then for the numerical solution u of ECS-II, we have*

$$\sum_{E\in\mathcal{E}} u_E \sum_{\sigma\in\sigma(E)} F_{E,\sigma} \geq \underline{\rho}\, |u|_1^2, \tag{14}$$

where $\underline{\rho} = \min_{K\in\mathcal{M}} \underline{\rho}_K$, and

$$|u|_1^2 = \sum_{K\in\mathcal{M}} \sum_{i=1}^{m_K} |u_{i+1} - u_i|^2 = \sum_{K\in\mathcal{M}} \|\delta U_K\|^2.$$

Here, $|u|_1$ represents the discrete H^1 semi-norm in edge-centered schemes.

Proof. Consider an arbitrary cell K, using the direction definition of flux $F_{\sigma_i} = F_{E_{i-1},\sigma_i} = -F_{E_i,\sigma_i}$, we can rearrange the items into

$$\sum_{E\in\mathcal{E}} u_E \sum_{\sigma\in\sigma(E)} F_{E,\sigma} = \sum_{K\in\mathcal{M}} \sum_{i=1}^{m_K} F_{\sigma_i} (u_{E_i} - u_{E_{i-1}}).$$

Substituting the numerical flux Eq. (4) into the above equation, and using the definition Eq. (3) and Lemma 2, we can get

$$\sum_{E\in\mathcal{E}} u_E \sum_{\sigma\in\sigma(E)} F_{E,\sigma} = \sum_{K\in\mathcal{M}} \delta U_K^T A_K\, \delta U_K^T \geq \sum_{K\in\mathcal{M}} \underline{\rho}_K \|\delta U_K\|^2 \geq \underline{\rho}\, |u|_1^2,$$

which completes the proof.

Multiplying both sides of Eq. (7) with u_E, summing it over all edge control volumes and recalling $g = 0$, we can get

$$\sum_{E\in\mathcal{E}} u_E \sum_{\sigma\in\sigma(E)} F_{E,\sigma} = \sum_{E\in\mathcal{E}} u_E \int_E f \,\mathrm{d}\boldsymbol{x}.$$

Here, we can see that the above proof implies that the matrix of the resulting linear system of ECS-II is SPD, then the existence and uniqueness of the scheme can be directly deduced by linear algebra. Moreover, by combining the coercivity result with a certain discrete Poincare inequality, we can obtain the stability result and discrete H^1 error estimate.

4.2. Two special cases of the scheme

4.2.1. The edge-centered scheme on triangular meshes

For triangular meshes, all edge-centered schemes satisfying linearity-preserving criterion reduce to the finite volume element method with Crouzeix-Raviart element (CR-FVEM) [21]. Therefore, the above results can also serve as the dual mesh construction and the convergence analysis for CR-FVEM.

For a triangular mesh $\mathcal{T}$, the dual mesh $\mathcal{T}^*$ is defined using the same process in section 2.2. For Crouzeix-Raviart element, the trial and test function spaces are chosen as

$$S_h = \{u \in L^2(\Omega) :\ u|_K \text{ is linear } \forall K \in \mathcal{T},\ u \text{ is continuous at all midpoints of edges in } \mathcal{T},\ u|_{\partial\Omega} = g\},$$

and

$$S_h^* = \{v \in L^2(\Omega) :\ v|_E \text{ is constant } \forall E \in \mathcal{T}^*,\ v|_{\partial\Omega} = 0\}.$$

The numerical scheme of CR-FVEM is to find $u \in S_h$, such that

$$-\sum_{E\in\mathcal{T}_h^*}\int_{\partial E}(\Lambda\,\nabla u)\cdot\boldsymbol{n}\ v\ \mathrm{d}s = \int_\Omega f\ v\ \mathrm{d}\boldsymbol{x}, \quad \forall v \in S_h^*. \tag{15}$$

Since the test function is piecewise constant on the dual mesh, the numerical scheme comes

$$-\int_{\partial E}(\Lambda\,\nabla u)\cdot\boldsymbol{n}\ \mathrm{d}s = \int_E f\ \mathrm{d}\boldsymbol{x}, \quad \forall E \in \mathcal{T}_h^*.$$

Then for CR-FVEM, the discrete flux across σ_i is given by

$$\hat{F}_{\sigma_i} = -\int_{\sigma_i}(\Lambda_K\,\nabla u)\cdot\boldsymbol{n}_{\sigma_i}\ \mathrm{d}s.$$

Since $u \in S_h$, which means that $u(\boldsymbol{x})$ is piecewise linear in CR-FVEM. And in edge centered scheme, recalling the definition Eq. (8) of numerical flux, according to the linearity-preserving property of edge-centered schemes, the discrete flux in CR-FVEM and edge-centered schemes are equal.

$$\hat{F}_{\sigma_i} = F_{\sigma_i}.$$

Then we can get that on triangular meshes, all edge-centered schemes satisfying linearity-preserving criterion are same, and they will reduce to CR-FVEM.

4.2.2. The edge-centered scheme on uniform orthogonal mesh

Consider the problem Eq. (1) with a constant scalar diffusion coefficient on the square domain $\Omega = [0,1]^2$. We will show that when solving the problem on a uniform mesh, the ECS-I will reduce to a rotated traditional five-point finite difference scheme.

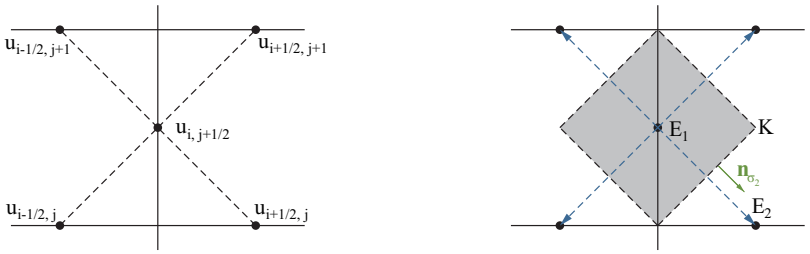

(a) stencil of FDM (b) stencil of ECS-I

Figure 2: Stencils of the finite difference scheme and ECS-I on the uniform mesh.

Consider a uniform mesh with size h. As shown in Figure 2a, in the finite difference scheme, unknowns are defined on edges denoted by $u_{i,j+\frac{1}{2}}$ and $u_{i+\frac{1}{2},j}$. Using the Talyor expansion and the symmetry, we can get a finite difference approximation writes

$$\triangle u_{i,j+\frac{1}{2}} = \frac{2}{h^2}\left(u_{i+\frac{1}{2},j+1} + u_{i+\frac{1}{2},j} + u_{i-\frac{1}{2},j+1} + u_{i-\frac{1}{2},j} - 4\,u_{i,j+\frac{1}{2}}\right) + \mathcal{O}(h^2).$$

The derivation the approximation of $\triangle u_{i+\frac{1}{2},j}$ is similar. Noting that Λ is a constant scalar, then we can get a finite difference scheme

$$-\Lambda\left(u_{i+\frac{1}{2},j+1} + u_{i+\frac{1}{2},j} + u_{i-\frac{1}{2},j+1} + u_{i-\frac{1}{2},j} - 4\,u_{i,j+\frac{1}{2}}\right) = \frac{h^2}{2}\,f_{i,j+\frac{1}{2}}. \tag{16}$$

The scheme can be seen as the rotation of the traditional five-point finite difference scheme, whose monotonicity and stability have been demonstrated.

Now we consider the ECS-I on the uniform orthogonal mesh. As shown in Figure 2b, for example, in a certain cell K, when we approximating the flux on σ_2, we have $|\sigma_2|\boldsymbol{n}_{\sigma_2} = \overrightarrow{E_1E_2}$. Then in the vector decomposition Eq. (9), we have $\alpha_- = -1, \alpha_+ = 0$. Therefore, the numerical flux on σ_2 is $F_{E_1,\sigma_2} = -F_{E_2,\sigma_2} = \Lambda_K(u(E_1) - u(E_2))$. On the other hand, noting that the measurement of each edge control volume is $\frac{h^2}{2}$ in the uniform mesh, when we compute the integral of $f(x)$ on the edge control volume E using numerical quadrature, the integral can be approximately regarded as the same as $\frac{h^2}{2}f(E)$. Then on the uniform orthogonal mesh, the ECS-I writes

$$\sum_{\bar{E}\in\mathcal{N}(E)} (u(E) - u(\bar{E})) = \frac{h^2}{2} f(E).$$

where $\mathcal{N}(E)$ represents all adjacent control volumes which have a common dual edge with E.

Here, we can get that the ECS-I on the uniform mesh is equal to the above finite difference scheme.

5. Numerical experiments

Here, we provide some numerical tests to show the performances of edge-centered schemes. The edge-centered schemes are compared with a so called nine point scheme (NPS) or diamond scheme [9] and the interpolation method is chosen as the second order interpolation (eLSW) suggested in [29].

In order to make the edge-centered and cell-centered schemes comparable, errors of the schemes are evaluated by following mesh-dependent norms. For a function U defined on edges or cells in mesh $\mathcal{M}$, the mesh-dependent L^2 and L^∞ norms are defined as following

$$\|U\|_2 = \sqrt{\sum_{\mathcal{A}} |\mathcal{A}| \, |U_{\mathcal{A}}|^2}, \qquad \|U\|_\infty = \max_{\mathcal{A}} |U_{\mathcal{A}}|, \tag{17}$$

where $\mathcal{A}$ represents each edge (for edge-centered schemes) or each cell (for cell-centered schemes) in the mesh $\mathcal{M}$ and $|\mathcal{A}|$ represents the measurement of the edge control volume or the cell respectively. Then the L^p $(p = 2, \infty)$ relative error of the numerical solution U is defined as following respectively

$$\mathrm{err}_p = \frac{\|U - U_{\mathrm{exact}}\|_p}{\|U_{\mathrm{exact}}\|_p}, \quad p = 2, \infty, \tag{18}$$

where U_{exact} is the vector of the values at the midpoint of each edge or the center of each cell of exact solution. The L^p $(p = 2, \infty)$ convergence rate is obtained by computing the following formula on each two successive meshes $\mathcal{M}_1$ and $\mathcal{M}_2$

$$\mathrm{rate}_p = -2\frac{\log \mathrm{err}_p(\mathcal{M}_1) - \log \mathrm{err}_p(\mathcal{M}_2)}{\log \mathrm{nkw}(\mathcal{M}_1) - \log \mathrm{nkw}(\mathcal{M}_2)}, \quad p = 2, \infty, \tag{19}$$

where $\mathrm{nkw}(\mathcal{M})$ represents the number of unknowns in the scheme, which is equal to the number of edge for edge-centered schemes and the number of cell for cell-centered schemes.

Following numerical examples are taken from the benchmark proposed at fifth conference on discretization schemes for anisotropic diffusion problems on general grids [30]. For ECS-II, by taking into account the accuracy and robustness, the parameter is chosen as $\gamma_K = 1$ if not mentioned.

5.1. Linearity-preserving

To verify the linearity-preserving property of the edge-centered schemes, we consider a problem on $\Omega = [0, 1]^2$ with identity diffusion coefficient and linear exact solution

$$\Lambda(x, y) = \begin{pmatrix} 1 & 0 \\ 0 & 1 \end{pmatrix}, \qquad u(x, y) = x + y + 1.$$

We conduct this test on the locally refined mesh, random polygonal mesh, skewed quadrilateral mesh, Kershaw mesh, triangular mesh and sin mesh. The meshes used in this test are shown in Figure 3. The results are presented in Table 1. The results show that the error of both schemes on all tested meshes close to machine precision, which means that both scheme reproduce the exact solution.

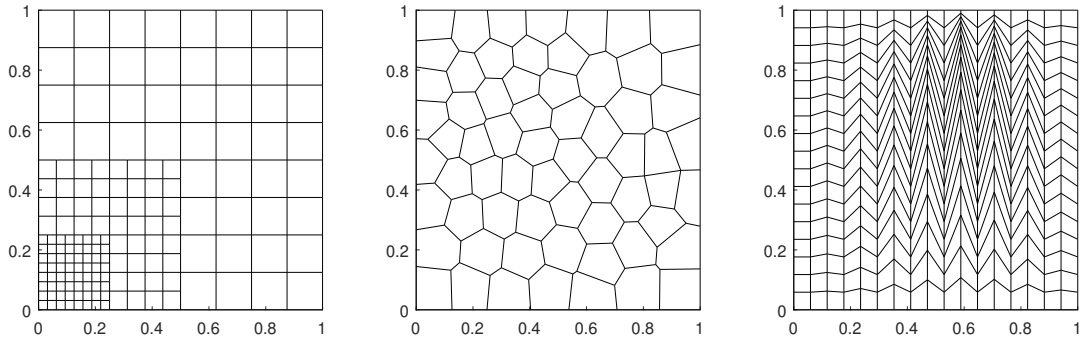

(a) locally refined mesh (b) random polygonal mesh (c) skewed quadrilateral mesh

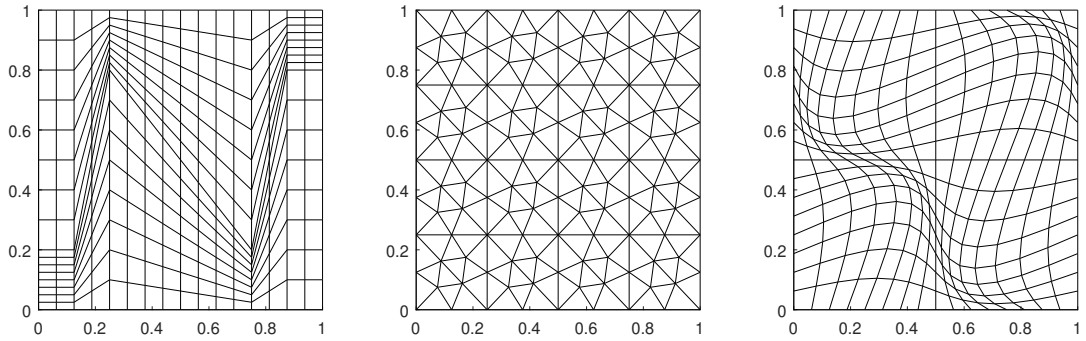

(d) Kershaw mesh (e) triangular mesh (f) sin mesh

Figure 3: Mesh types used in numerical experiments

5.2. Unstructured meshes

Consider the problem on $\Omega = [0,1]^2$ with constant anisotropic diffusion tensor and the exact solution given as follows

$$\Lambda(x,y) = \begin{pmatrix} 1.5 & 0.5 \\ 0.5 & 1.5 \end{pmatrix}, \qquad u(x,y) = \sin((x-1)(y-1)) - (x-1)^3 (y-1)^2.$$

The locally refined mesh and the random polygonal mesh shown in Figure 3 are used here. On the locally refined mesh, the errors of ECS-I are $\mathrm{err}_2 = 0.99 \times 10^{-3}, \mathrm{err}_\infty = 1.42 \times 10^{-3}$, and the errors of ECS-II are $\mathrm{err}_2 = 1.66 \times 10^{-3}, \mathrm{err}_\infty = 2.16 \times 10^{-3}$. On the random polygonal mesh, the errors of ECS-I are $\mathrm{err}_2 = 4.62 \times 10^{-3}, \mathrm{err}_\infty = 7.02 \times 10^{-3}$, and the errors of ECS-II are $\mathrm{err}_2 = 5.37 \times 10^{-3}, \mathrm{err}_\infty = 9.37 \times 10^{-3}$. The numerical solution u and the error function $u - u_{\mathrm{exact}}$ of both schemes on corresponding meshes are shown in Figure 4. One can see that edge-centered schemes can handle the unstructured mesh well.

		mesh (a)	mesh (b)	mesh (c)	mesh (d)	mesh (e)	mesh (f)
ECS-I	err_2	3.52e-16	4.73e-16	3.72e-15	2.24e-15	9.28e-16	5.61e-16
	err_∞	6.80e-16	9.06e-16	1.36e-14	7.28e-15	1.51e-15	1.35e-15
ECS-II	err_2	1.74e-15	7.58e-16	1.97e-15	2.12e-15	5.28e-16	1.19e-15
	err_∞	3.02e-15	1.21e-15	5.68e-15	4.61e-15	1.21e-15	2.24e-15

Table 1: Errors of two edge-centered schemes for linear solution on different meshes.

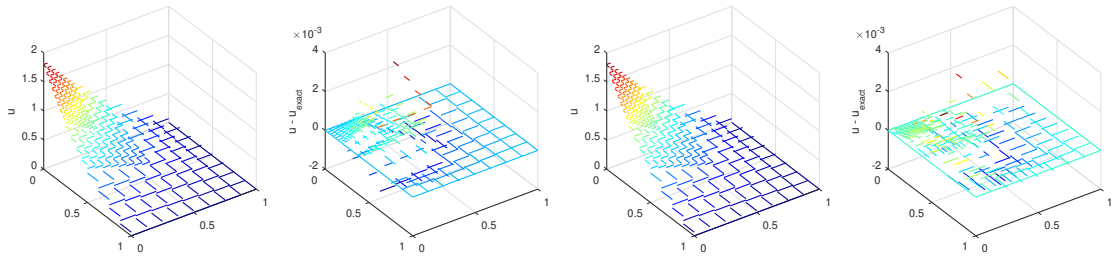

(a) solution of ECS-I (b) error of ECS-I (c) solution of ECS-II (d) error of ECS-II

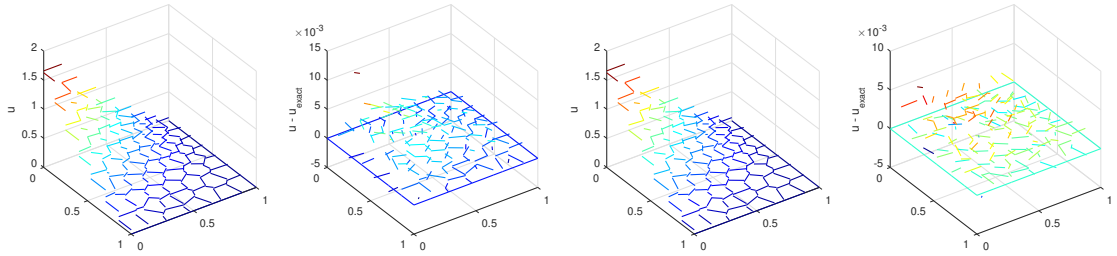

(e) solution of ECS-I (f) error of ECS-I (g) solution of ECS-II (h) error of ECS-II

Figure 4: Numerical solutions and error functions of two edge-centered schemes on two meshes

5.3. Accuracy of edge-centered schemes

To test the accuracy of edge-centered schemes on distorted meshes, we consider a simple problem with diffusion tensor and exact solution given as follows

$$\Lambda(x,y) = \begin{pmatrix} 1.5 & 0.5 \\ 0.5 & 1.5 \end{pmatrix}, \qquad u(x,y) = 16\,x\,(1-x)\,y\,(1-y).$$

A family of skewed quadrilateral meshes shown in Figure 3c are used. The distortion of meshes is the main difficulty in this example. The results are presented in Table 2 and Table 3. On such skewed meshes, NPS cannot attain optimal order may because of the loss of precision in interpolation step, but edge-centered schemes can attain optimal convergence order.

mesh size	NPS			ECS-I			ECS-II		
	nkw	err_2	order	nkw	err_2	order	nkw	err_2	order
17×17	289	1.49e-02	*	612	2.21e-02	*	612	2.32e-02	*
34×34	1156	4.06e-02	-1.44	2380	5.64e-03	2.01	2380	6.01e-03	1.99
51×51	2601	2.76e-02	0.96	5304	2.51e-03	2.01	5304	2.70e-03	2.00
68×68	4624	1.88e-02	1.33	9384	1.42e-03	2.01	9384	1.52e-03	2.01
85×85	7225	1.34e-02	1.51	14620	9.07e-04	2.01	14620	9.75e-04	2.01
102×102	10404	1.00e-02	1.61	21012	6.30e-04	2.01	21012	6.77e-04	2.01

Table 2: L^2 relative error and convergence rate of different schemes on skewed quadrilateral meshes

mesh size	NPS			ECS-I			ECS-II		
	nkw	E_∞	order	nkw	E_∞	order	nkw	E_∞	order
17×17	289	2.35e-02	*	612	5.80e-02	*	612	4.98e-02	*
34×34	1156	6.50e-02	-1.47	2380	1.49e-02	2.00	2380	1.30e-02	1.97
51×51	2601	4.56e-02	0.87	5304	6.64e-03	2.02	5304	5.83e-03	2.00
68×68	4624	3.18e-02	1.25	9384	3.73e-03	2.02	9384	3.29e-03	2.01
85×85	7225	2.31e-02	1.44	14620	2.39e-03	2.01	14620	2.11e-03	2.00
102×102	10404	1.74e-02	1.56	21012	1.66e-03	2.01	21012	1.47e-03	2.00

Table 3: L^∞ relative error and convergence rate of different schemes on skewed quadrilateral meshes

5.4. Anisotropic diffusion problem

In practical applications, we often encounter the problems with distorted meshes and anisotropy simultaneously. To test the accuracy of schemes for anisotropic diffusion problems, we consider

$$\Lambda(x,y) = \begin{pmatrix} 1 & 0 \\ 0 & \delta \end{pmatrix}, \qquad u(x,y) = \sin(2\pi x)\, \exp(-\frac{2\pi}{\sqrt{\delta}} y).$$

We take $\delta = 10^5$ then the problem has strong anisotropy. A sequence of Kershaw meshes shown in Figure 3d are used. Kershaw mesh is recognized as challenging because of its distortion. The results are shown in Table 4 and Table 5, which states that edge-centered schemes work well in this experiment.

5.5. Heterogeneous diffusion problem

Heterogeneous is represented by the discontinuity of diffusion tensor in the model, which is very common in practical calculations. To test the ability of schemes for handling heterogeneous problems, we divide the domain $\Omega = [0,1]^2$ into four parts, the diffusion tensor and the solution on each part is chosen as

$$\Lambda = \begin{pmatrix} a_1 & 0 \\ 0 & a_2 \end{pmatrix}, \qquad u(x,y) = \alpha\, \sin(2\pi x)\, \sin(2\pi y),$$

mesh size	NPS			ECS-I			ECS-II		
	nkw	err_2	order	nkw	err_2	order	nkw	err_2	order
4×4	16	2.79e-01	*	40	2.93e-01	*	40	1.85e-01	*
8×8	64	8.08e-02	1.79	144	5.82e-02	2.52	144	5.68e-02	1.85
16×16	256	4.14e-02	0.96	544	1.39e-02	2.16	544	1.85e-02	1.68
32×32	1024	5.70e-02	-0.46	2112	3.42e-03	2.06	2112	5.09e-03	1.91
64×64	4096	1.34e-02	2.08	8320	8.53e-04	2.03	8320	1.31e-03	1.98
128×128	16384	3.11e-03	2.11	33024	2.13e-04	2.01	33024	3.30e-04	2.00

Table 4: L^2 relative error and convergence rate of different schemes for the anistropic problem

mesh size	NPS			ECS-I			ECS-II		
	nkw	E_∞	order	nkw	E_∞	order	nkw	E_∞	order
4×4	16	3.60e-01	*	40	4.16e-01	*	40	2.81e-01	*
8×8	64	1.29e-01	1.48	144	8.29e-02	2.52	144	8.49e-02	1.87
16×16	256	1.05e-01	0.30	544	1.99e-02	2.15	544	3.23e-02	1.46
32×32	1024	2.48e-01	-1.24	2112	4.88e-03	2.07	2112	9.47e-03	1.81
64×64	4096	7.84e-02	1.66	8320	1.21e-03	2.03	8320	2.52e-03	1.93
128×128	16384	2.58e-02	1.60	33024	3.03e-04	2.01	33024	6.47e-04	1.97

Table 5: L^∞ relative error and convergence rate of different schemes for the anistropic problem

where

$$\begin{cases} a_1 = 10, & a_2 = 0.01, & \alpha = 0.1 & \text{for} & 0 < x \leq 0.5, & 0 < y \leq 0.5, \\ a_1 = 0.1, & a_2 = 100, & \alpha = 10 & \text{for} & 0.5 < x < 1, & 0 < y \leq 0.5, \\ a_1 = 100, & a_2 = 0.1, & \alpha = 0.01 & \text{for} & 0 < x \leq 0.5, & 0.5 < y < 1, \\ a_1 = 0.01, & a_2 = 10, & \alpha = 100 & \text{for} & 0.5 < x < 1, & 0.5 < y < 1. \end{cases}$$

A sequence of triangular meshes shown in Figure 3e are used. The results are shown in Table 6 and Table 7. One can see that results of both edge-centered schemes are same on triangular meshes. This is consistent with our previous theoretical results i.e. both schemes are equivalent to CR-FVEM on triangular meshes. Though the relative error of edge-centered schemes are big, edge-centered schemes presents the optimal order.

5.6. Robustness under the heterogeneous rotating anisotropy problem

Finally, noting that we introduce a stabilization parameter γ_K in ECS-II, we want to verify the robustness of the ECS-II with respect to γ_K. Here we choose the problem as

$$\Lambda(x, y) = \frac{1}{x^2 + y^2} \begin{pmatrix} \delta\, x^2 + y^2 & (\delta - 1)\, x\, y \\ (\delta - 1)\, x\, y & x^2 + \delta\, y^2 \end{pmatrix}, \qquad u(x, y) = sin(\pi\, x)\, \sin(\pi\, y).$$

mesh size	NPS			ECS-I			ECS-II		
	nkw	err_2	order	nkw	err_2	order	nkw	err_2	order
2×2	56	4.76e-01	*	92	9.33e+01	*	92	9.33e+01	*
4×4	224	1.29e-01	1.89	352	1.63e+01	2.60	352	1.63e+01	2.60
8×8	896	2.64e-02	2.28	1376	3.68e+00	2.18	1376	3.68e+00	2.18
16×16	3584	5.88e-03	2.17	5440	7.45e-01	2.32	5440	7.45e-01	2.32
32×32	14336	1.31e-03	2.16	21632	1.59e-01	2.24	21632	1.59e-01	2.24
64×64	57344	2.88e-04	2.19	86272	3.73e-02	2.09	86272	3.73e-02	2.09

Table 6: L^2 relative error and convergence rate of different schemes for the heterogeneous problem

mesh size	NPS			ECS-I			ECS-II		
	nkw	E_∞	order	nkw	E_∞	order	nkw	E_∞	order
2×2	56	5.65e-01	*	92	7.67e+01	*	92	7.67e+01	*
4×4	224	2.85e-01	0.99	352	2.44e+01	1.71	352	2.44e+01	1.71
8×8	896	8.61e-02	1.73	1376	5.67e+00	2.14	1376	5.67e+00	2.14
16×16	3584	2.65e-02	1.70	5440	1.22e+00	2.24	5440	1.22e+00	2.24
32×32	14336	7.58e-03	1.80	21632	2.94e-01	2.06	21632	2.94e-01	2.06
64×64	57344	2.00e-03	1.93	86272	7.26e-02	2.02	86272	7.26e-02	2.02

Table 7: L^∞ relative error and convergence rate of different schemes for the heterogeneous problem

The parameter is chosen as $\delta = 10^{-3}$ here. A sequence of sin meshes shown in Figure 3f are used.

This problem is universally considered as challenging [31, 32]. Here we test the problem using the schemes mentioned above under a wide range of parameter γ_K. The result is shown in Figure 5. From the figure on can see that both edge-centered schemes under different parameters are all second order. In this example, a small γ_K will only make error increase, but makes no influence to the convergence order.

6. Conclusion

In this paper, we propose a family of edge-centered schemes (ECS-I and ECS-II) for two-dimensional diffusion problems on unstructrued meshes. The schemes takes into account arbitrary heterogeneous anisotropic diffusion problems. Particularly, ECS-II is proved to be symmetric and coercive under general assumptions. Sufficient numerical tests using unstructured and severely distorted meshes and various of (continuous or discontinuous) anisotropic diffusion tensors show the accuracy and robustness of schemes.

The extension of present schemes to 3D polyhedral meshes is not so easy but still possible, which constitute the topics of our future work. Further, constructing an edge-centered scheme which satisfies discrete maximum principle is also our future work.

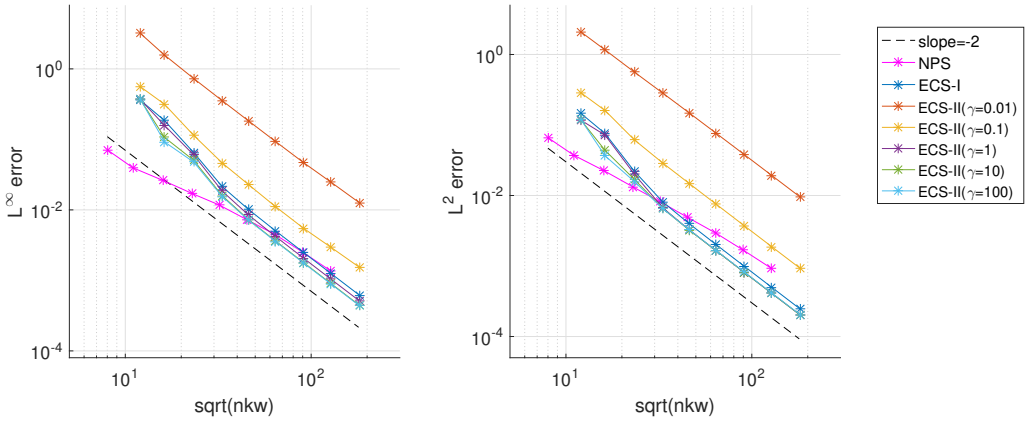

Figure 5: L^2 and L^∞ relative errors versus nkw for the schemes under different parameters.

References

[1] H. Versteeg, W. Malalasekera, An Introduction to Computational Fluid Dynamics, Prentice Hall, 2007.

[2] R. Leveque, Finite Volume Methods for Hyperbolic Problems: Bibliography, Cambridge University Press, 2013.

[3] T. de M. Cavalcante, F. Contreras, P. Lyra, D. de Carvalho, A multipoint flux approximation with diamond stencil finite volume scheme for the two-dimensional simulation of fluid flows in naturally fractured reservoirs using a hybrid-grid method, Int. J. Numer. Meth. Fluids 92 (10) (2020) 1322–1351. doi:10.1002/fld.4829.

[4] M. Schneider, D. Gläser, B. Flemisch, R. Helmig, Comparison of finite-volume schemes for diffusion problems, Oil Gas Sci. Technol. – Rev. IFP Energies nouvelles 73 (2018) 82. doi:10.2516/ogst/2018064.

[5] F. Contreras, P. Lyra, M. Souza, D. Carvalho, A cell-centered multipoint flux approximation method with a diamond stencil coupled with a higher order finite volume method for the simulation of oil-water displacements in heterogeneous and anisotropic petroleum reservoirs, Comput. Fluids 127 (2016) 1–16. doi:10.1016/j.compfluid.2015.11.013.

[6] P. Markowich, C. Ringhofer, C. Schmeiser, Semiconductor Equations, Springer Vienna, Vienna, 1990. doi:10.1007/978-3-7091-6961-2.

[7] I. Aavatsmark, T. Barkve, B. O. ., T. Mannseth, Discretization on unstructured grids for inhomogeneous, anisotropic media. I. Derivation of the methods, SIAM J. Sci. Comput. 19 (5) (1998) 1700–1716. doi:10.1137/S1064827595293582.

[8] I. Aavatsmark, An introduction to multipoint flux approximations for quadrilateral grids, Comput. Geosci. 6 (3-4) (2002) 405–432. doi:10.1023/A:1021291114475.

[9] D. Li, H. Shui, M. Tang, On the finite difference scheme of two-dimensional parabolic equation in a non-rectangular mesh, J. Numer. Methods Comput. Appl 1 (4) (1980) 217–224.

[10] Y. Coudière, J.-P. Vila, P. Villedieu, Convergence rate of a finite volume scheme for a two-dimensional convection-diffusion problem, M2AN Math. Model. Numer. Anal. 33 (3) (1999) 493–516. doi:10.1051/m2an:1999149.

[11] M. Edwards, Unstructured, control-volume distributed, full-tensor finite-volume schemes with flow based grids, Comput. Geosci. 6 (3-4) (2002) 433–452. doi:10.1023/A:1021243231313.

[12] M. Edwards, Unstructured, control-volume distributed, full-tensor finite-volume schemes with flow based grids, Comput. Geosci. 6 (3-4) (2002) 433–452. doi:10.1023/A:1021243231313.

[13] J. Wu, Z. Gao, Z. Dai, A vertex-centered linearity-preserving discretization of diffusion problems on polygonal meshes, Int. J. Numer. Methods Fluids 81 (3) (2016) 131–150. doi:10.1002/fld.4178.

[14] F. Brezzi, K. Lipnikov, M. Shashkov, Convergence of the mimetic finite difference method for diffusion problems on polyhedral meshes, SIAM J. Numer. Anal. 43 (5) (2005) 1872–1896. doi:10.1137/040613950.

[15] F. Brezzi, K. Lipnikov, V. Simoncini, A family of mimetic finite difference methods on polygonal and polyhedral meshes, Math. Models Methods Appl. Sci. 15 (10) (2005) 1533–1551. doi:10.1142/S0218202505000832.

[16] K. Lipnikov, G. Manzini, M. Shashkov, Mimetic finite difference method, J. Comput. Phys. 257 (2014) 1163–1227. doi:https://doi.org/10.1016/j.jcp.2013.07.031.

[17] J. Droniou, Finite volume schemes for diffusion equations: introduction to and review of modern methods, Math. Models Methods Appl. Sci. 24 (8) (2014) 1575–1619. doi:10.1142/S0218202514400041.

[18] F. Hermeline, A finite volume method for the approximation of diffusion operators on distorted meshes, J. Comput. Phys. 160 (2) (2000) 481–499. doi:10.1006/jcph.2000.6466.

[19] B. Andreianov, F. Boyer, F. Hubert, Discrete duality finite volume schemes for Leray-Lions-type elliptic problems on general 2D meshes, Numer. Methods Partial Differ. Eqs. 23 (1) (2007) 145–195. doi:10.1002/num.20170.

[20] Y. Wang, T. Yang, L. Chang, An edge-centered scheme for anisotropic diffusion problems with discontinuities on distorted quadrilateral meshes, J. Comput. Sci. (2022) 101832doi:10.1016/j.jocs.2022.101832.

[21] P. Chatzipantelidis, A finite volume method based on the Crouzeix-Raviart element for elliptic PDE's in two dimensions, Numer. Math. 82 (3) (1999) 409–432. doi:10.1007/s002110050425.

[22] I. Rees, I. Masters, A. Malan, R. Lewis, An edge-based finite volume scheme for saturated–unsaturated groundwater flow, Comput. Methods Appl. Mech. Engrg. 193 (42/44) (2004) 4741–4759. doi:10.1016/j.cma.2004.04.003.

[23] R. Sevilla, M. Giacomini, A. Huerta, A face-centred finite volume method for second-order elliptic problems, Int. J. Numer. Methods Engrg. 115 (8) (2018) 986–1014. doi:10.1002/nme.5833.

[24] L. Vieira, M. Giacomini, R. Sevilla, A. Huerta, A second-order face-centred finite volume method for elliptic problems, Comput. Methods Appl. Mech. Engrg. 358 (2020) 112655, 23. doi:10.1016/j.cma.2019.112655.

[25] R. Sevilla, M. Giacomini, A. Huerta, A locking-free face-centred finite volume (FCFV) method for linear elastostatics, Comput. Struct. 212 (2019). doi:10.1016/j.compstruc.2018.10.015.

[26] J. Vila-Pérez, M. Giacomini, R. Sevilla, A. Huerta, A non-oscillatory face-centred finite volume method for compressible flows, Comput. Fluids 235 (2022) 105272. doi:10.1016/j.compfluid.2021.105272.

[27] M. Giacomini, R. Sevilla, A second-order face-centred finite volume method on general meshes with automatic mesh adaptation, Int. J. Numer. Methods Engrg. 121 (23) (2020) 5227–5255. doi:10.1002/nme.6428.

[28] Q. Dong, S. Su, J. Wu, Analysis of the decoupled and positivity-preserving DDFV schemes for diffusion problems on polygonal meshes, Adv. Comput. Math. 46 (2) (2020) 12. doi:10.1007/s10444-020-09748-4.

[29] S. Miao, J. Wu, A nonlinear correction scheme for the heterogeneous and anisotropic diffusion problems on polygonal meshes, J. Comput. Phys. 448 (2022) 110729. doi:10.1016/j.jcp.2021.110729.

[30] R. Herbin, F. Hubert, Benchmark on discretization schemes for anisotropic diffusion problems on general grids, Finite Volumes for Complex Applications V (2008) 659–692.

[31] C. L. Potier, Schéma volumes finis monotone pour des opérateurs de diffusion fortement anisotropes sur des maillages de triangles non structurés, C. R. Acad. Sci. Paris, Ser. I 341 (12) (2005) 787–792. doi:10.1016/j.crma.2005.10.010.

[32] K. Terekhov, B. Mallison, H. Tchelepi, Cell-centered nonlinear finite-volume methods for the heterogeneous anisotropic diffusion problem, J. Comput. Phys. 330 (2017) 245–267. doi:10.1016/j.jcp.2016.11.010.